

# Interplay among Bilayer PseudoSpin Field-Effect Transistor (BiSFET) Performance, BiSFET Scaling and Condensate Strength

Xuehao Mou, Leonard F. Register and Sanjay K. Banerjee

Microelectronics Research Center and Department of ECE, The University of Texas at Austin  
10100 Burnet Road, Building 160, Austin, Texas 78758, United States, Email: xmou@utexas.edu

**Abstract**—It has been proposed that superfluid excitonic condensates may be possible in dielectrically separated graphene layers or other two-dimensional materials. This possibility was the basis for the proposed ultra-low power Bilayer pseudoSpin Field-effect Transistor (BiSFET). Previously, we developed an atomistic tight-binding quantum transport simulator, including the non-local exchange interaction, and used it to demonstrate the essential excitonic superfluid transport physics which underlies the proposed BiSFET in presence of such a condensate. Here we report on extension of that work to analyze dependencies on device scaling and the condensate strength of BiSFET performance and required device parameters including interlayer conductance, and critical current and voltage.

**Keywords**—graphene, BiSFET, exciton condensate, Fock exchange, critical current and voltage, quantum transport

## I. INTRODUCTION

The Bilayer pseudoSpin Field-Effect Transistor (BiSFET) is an ultra-low power “beyond-CMOS” device proposal based on the possibility of interlayer electron-hole exciton condensation above room temperature in dielectrically separated graphene layers [1]. Such condensates have been observed in III-V double quantum wells under cryogenic temperatures ( $\sim$ mK) [2-4] and explained theoretically [5]. By extension of the latter theory, exciton condensation, perhaps above room temperature, was predicted to be possible between two graphene layers, one n-type and one p-type, coupled via the interlayer many-body Fock exchange interaction [6,7]. Analogous systems incorporating monolayers of transition metal dichalcogenides also are being considered [8]. Notably, the phase-coherent state between the two layers can be thought of as a pseudospin in the “which layer” degree of freedom with magnitude and phase, from which the “BiSFET” moniker is derived. Creating any of these systems experimentally is extremely challenging and requires a low-dielectric environment, however, and to date the theory has been neither proven nor disproven experimentally.

Given potentially transformative applications, we have extended our efforts to better understand the properties of the condensate through equilibrium and perturbative transport models [9,10], and most recently via the development and application of an atomistic tight-binding quantum transport

simulator self-consistently including the non-local exchange interaction [11]. The latter is intended to address not the possibility of condensate formation, but rather transport physics in the presence of such a condensate, which can be realized and controlled easily enough in simulation. We already have exhibited steady-state interlayer current enhanced by orders of magnitude, up to near the Landauer-Büttiker ballistic limit of the leads in the presence of the condensate, but only up to critical interlayer current  $I_{\text{crit}}$  and associated voltage,  $V_{\text{crit}}$  [11,12]. Beyond  $V_{\text{crit}}$ , results are consistent with the expected collapse of the DC current and onset of rapid AC oscillations ( $\sim$ 10 GHz in this case) as for a Josephson junction. (Above  $V_{\text{crit}}$ , which is associated with a pseudospin phase of  $\pi/2$ , no steady-state result can be found in our iterative self-consistent calculations, and the pseudospin phase rotates through  $2\pi$  periodically with iteration while the pseudospin magnitude remains constant.) Moreover, we also have exhibited nano-scale condensates and sub-thermal-voltage (sub  $k_B T/q$ )  $V_{\text{crit}}$  [11,12], which would allow for BiSFET switching energies of a few tens of zJ ( $1 \text{ zJ} = 10^{-21} \text{ J}$ ), two or more orders of magnitude below end-of-the-roadmap CMOS.

In this work, we have employed this simulation tool to model the dependencies of  $I_{\text{crit}}$  and  $V_{\text{crit}}$  and the interlayer ON-state conductance  $G_{\text{il}}$  on the device size and strength of the condensate, to illustrate trends relevant to experimentalists, to provide parameters for compact models for subsequent BiSFET circuit simulation, and to lay a foundation for other possible devices based on the same transport physics [13].

## II. SIMULATION METHODS

The simulated structure is shown in Fig. 1. Two graphene layers are coupled by the interlayer Fock exchange interaction and weak bare (not exchange-mediated) coupling within a channel of length  $L$  and infinite width. The two layers are connected to perfectly injecting and absorbing semi-infinite leads, characterized by voltages,  $V_{\text{TL}}$ ,  $V_{\text{BL}}$ ,  $V_{\text{TR}}$  and  $V_{\text{BR}}$ , defining the Fermi levels for injected carriers. The occupation probability for injected carriers is further characterized by the simulation temperature  $T$ . Bottom and top layers are necessarily oppositely doped (likely electrostatically via external gates in practice). The graphene layers are separated

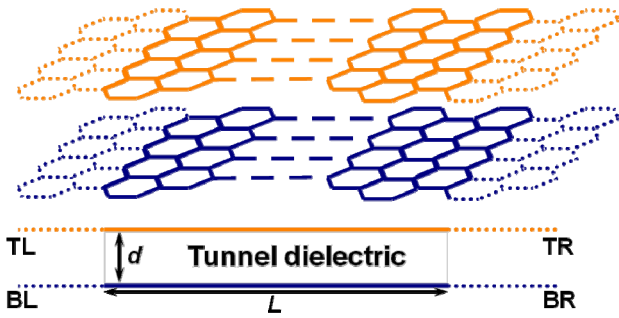


Fig. 1. Simulated dielectrically separated graphene layers with perfectly injecting and absorbing leads, with parameters as described and provided in the text. The two layers are equally and oppositely doped (and likely would be electrostatically via gates of fixed voltage not shown).

by the interlayer dielectric by a distance  $d$ . The effective dielectric environment including dielectrics above, below and between the layers, plus free-carrier screening (which is reduced self-consistently in the presence of the condensate [7]) are all modeled via an effective dielectric constant  $\epsilon_r$ . For simplicity, bare coupling through the dielectric is modeled as vertical A sub-lattice to A sub-lattice only (where for more complicated patterns, such contributions should dominate [10] with a coupling strength of  $V_b$ ).

In this work we set  $d = 1$  nm, and the bottom and top layer equilibrium carrier concentration are, respectively,  $p = n = 6 \times 10^{12}$  cm $^{-2}$  (corresponding to a  $\sim \pm 0.25$  eV electrostatic potential energy shifts, respectively, of the Dirac points relative to the equilibrium Fermi level  $E_F$ ).  $T$  is taken to be 300 K and  $V_b$  is taken to be 0.5 meV ( $\sim$ three orders of magnitude below intra-layer coupling potentials), except when calculating the bulk condensate critical temperature  $T_{c,\text{bulk}}$ —the temperature at which the condensate collapses—using the formalism in [9]. The applied voltages are taken to be of the form  $V_{\text{TL}} = -V_{\text{BL}} = V_{\text{il}}/2$  and  $V_{\text{TR}} = V_{\text{BR}} = 0$ . This biasing is much like that of the BiSFET except that  $V_{\text{TR}}$  and  $V_{\text{BR}}$  are left floating in the latter case. However, as will be seen, the condensate blocks current flow into either the TR or BR leads independent of  $V_{\text{TL}}$  and  $V_{\text{BL}}$ , so the difference is of little significance.  $\epsilon_r$  and  $L$  are taken to be adjustable parameters.

### III. SIMULATION RESULTS

#### A. Condensate Strength

The non-local interlayer Fock exchange interaction is just the interlayer density matrix as a function of atomic sites in the top and bottom layers, multiplied by the electrostatic interaction between those sites. The latter is modeled as Coulombic within effective dielectric environment characterized by  $\epsilon_r$  [9]. The larger the  $\epsilon_r$ , the weaker the Coulombic interaction and, thus, the weaker the self-consistently obtained exchange interaction and condensate, if any. With a sufficiently small  $\epsilon_r$ , the interlayer exchange interaction will produce an energy anti-crossing/band gap  $E_g$  centered around where the bottom layer valence band and top layer conduction band otherwise would have crossed, and about the Fermi level with  $n = p$ , with interlayer coherent

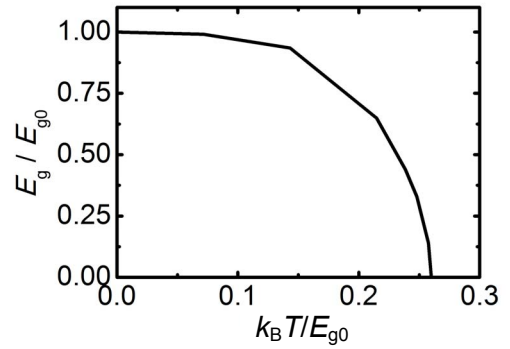


Fig. 2. Bulk condensate anti-crossing/band gap  $E_g$  vs. temperature  $T$ , normalized to the zero temperature band gap energy  $E_{g0}$ . That shown is for  $\epsilon_r = 2.5$  with a corresponding  $E_{g0}$  of 180 meV, but the result is essentially independent of  $\epsilon_r$  or  $d$  [9]. The condensate collapses at a critical temperature of  $4k_B T_{c,\text{bulk}} \approx E_{g0}$ . Thus,  $T_{c,\text{bulk}}$  serves as a measure of the nominal bulk condensate strength.

states near the anti-crossing, which are (necessarily) mostly occupied below and mostly empty above, producing a strong interlayer density matrix—pseudospin/exciton condensate—and, thus, a strong interlayer exchange interaction, all in a self-consistent manner. For weak bare coupling as here, the relation between the 0 K band gap/anti-crossing  $E_g(T=0) \equiv E_{g0}$  and the critical temperature for collapse of the bulk condensates is given by  $4k_B T_{c,\text{bulk}} \approx E_{g0}$ , as shown in Fig. 2, essentially independent of  $E_{g0}$  [9]. Thus,  $T_{c,\text{bulk}}$  can be used as a measure of the nominal strength of the bulk condensate. For dielectric constants of  $\epsilon_r = 2.2, 2.5$  and  $3.0$ ,  $T_{c,\text{bulk}}$  is  $\sim 650$  K,  $\sim 540$  K, and  $\sim 400$  K, respectively.

#### B. Sub-Critical Interlayer Conductance

While the weak bare coupling  $V_b$  considered here has a negligible effect on the condensate strength, it is indispensable for interlayer transport. However, the interlayer current is greatly enhanced by the condensate. Specifically, the interlayer current between any two atomic sites is proportional to the bare interlayer coupling strength  $V_b$  between that site pair, the pseudospin magnitude for that site pair, and the sine of the pseudospin phase  $\theta$  for that pair (the latter two via the Fock interaction) [11,12]. Importantly, the pseudospin amplitude is largely bias-independent, and the pseudospin phase is bias dependent but roughly uniform along the channel [12]. The sine of the calculated interlayer pseudospin phase  $\theta$  and the associated interlayer current  $I_{\text{il}}$ , both vs. the interlayer voltage  $V_{\text{il}}$  are plotted in Fig. 3(a) and (b), respectively, for  $T_{c,\text{bulk}} = 540$  K.  $\sin(\theta)$  and, therefore,  $I_{\text{il}}$  are linearly dependent on  $V_{\text{il}}$ . The corresponding constant interlayer conductances  $G_{\text{il}} = I_{\text{il}}/V_{\text{il}}$  are shown in Fig. 4.  $G_{\text{il}}$  increases with increasing channel lengths at first and then saturates to a constant, reflecting the formation of the condensate in the nano-scale channel.

The weaker the bulk condensate (the lower  $T_{c,\text{bulk}}$ ) the longer the channel has to be to fully form the condensate. The saturated  $G_{\text{il}}$  per unit width in all cases (and independent of  $V_b$  [11,12]), however, is approximately 155 S/cm ( $R_{\text{il}} \approx 64.5$   $\Omega$ - $\mu\text{m}$ ), which is about 75% of the Landauer-Büttiker ballistic limit for lead-limited transport. Still even an incompletely

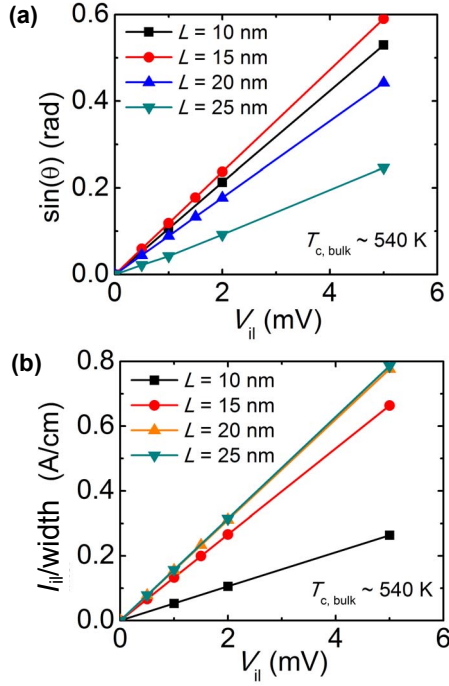


Fig. 3. (a) Sine of interlayer-current associated pseudospin phase  $\theta$  (b) interlayer current  $I_{il}$  vs. interlayer voltage  $V_{il}$  relations for a condensate of  $T_{c,bulk} \approx 540$  K ( $\epsilon_r = 2.5$ ). Both the sine of the pseudospin phase and the interlayer current vary linearly on  $V_{il}$ .

formed condensate provides greatly enhanced (multi orders of magnitude)  $G_{il}$ .

### C. Critical Current & Voltage

The critical interlayer voltage  $V_{crit}$  and corresponding interlayer critical current  $I_{crit}$  can be obtained readily by extrapolating the  $\sin(\theta)$  as a function of  $V_{il}$  relation to its maximum possible value of unity [12]. Note again that unlike the critical temperature, the critical current and voltage are not associated with breakdown of the condensate, only the transition from a DC to AC interlayer current, with the latter being so high in frequency here that it would be filtered out in most circuits. ( $I_{crit}$  and  $V_{crit}$  also can be localized above and below via direct iterative calculations. However, as  $V_{crit}$  is approached, the iterative calculations take progressively longer to stabilize below and to rotate above, making exact determination in this latter way computationally inefficient.)

The critical current dependencies on bulk condensate strength and the channel length  $L$  are presented in Fig. 5. Allowing for incomplete condensate formation near the edges of the channel and thus an effective channel length  $L_{eff}$  somewhat less than  $L$ ,  $I_{crit}$  increases roughly linearly with the channel area. It is the critical current *density* in terms of  $L_{eff}$  that is a roughly constant function for a given  $V_b$ , as expected from the perturbative calculations [9,10]. However, both  $L_{eff}$  for a given  $L$  and the critical current density in terms of  $L_{eff}$  decrease with decreasing condensate strength.

The  $V_{crit}$  dependencies on bulk condensate strength and  $L$  are presented in Fig. 6. For longer channels with saturated  $G_{il}$ ,  $V_{crit}$  increases with increasing  $L_{eff}$  and associated  $I_{crit}$ .

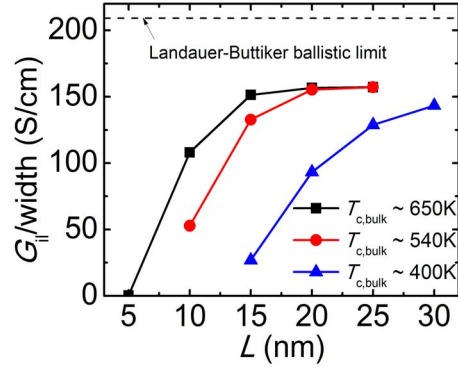


Fig. 4. Extracted voltage-independent interlayer conductances  $G_{il} = I_{il}/V_{il}$ . For condensate strengths of  $T_{c,bulk} \sim 650$  K and 540 K,  $G_{il}$  saturates to about 75% of the Landauer-Büttiker limit for lead-limited transport with full formation of the condensate in the channel, and  $G_{il}$  for  $T_{c,bulk} \sim 400$  K appears headed to the same. The weaker the bulk condensate, the longer the channel required for full formation. Still even an incompletely formed condensate provides greatly enhanced (multi orders of magnitude)  $G_{il}$ .

However, for shorter channels where  $G_{il}$  decreases with decreasing  $L_{eff}$ ,  $V_{crit}$  reaches a minimum and then begins to increase with decreasing  $L$ . The weaker the bulk condensate, the larger the value  $L$  at which this minimum is reached.

### D. Current Distribution

Intra- and inter-layer current distributions are as shown in Fig. 7 for a  $T_{c,bulk} = 540$  K condensate, where the position along the channel has been normalized with respect to  $L$ . With  $V_{TL} = -V_{BL} = V_{il}/2$  and  $V_{TR} = V_{BR} = 0$ , there is, of course, an intra-layer bias as well as in interlayer bias. Nevertheless, the intra-layer current flow to the grounded right-side leads TR and BR decays rapidly with increasing channel length. Current flow from left to right is blocked by the condensate band gap opened up about the Fermi level. However, the interlayer current flows throughout the condensate region, consistent with the condensates being able to support a roughly constant critical current density, although some skewing of the current density to the left occurs with increasing channel length. Blocking of intra-layer current flow *completely through* the condensate region while intra- (and inter-) layer current flow remains *delocalized throughout* the condensate region may seem contradictory. However, the

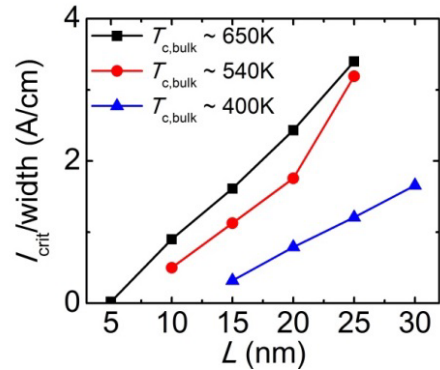


Fig. 5. Extracted critical currents for different channel lengths and bulk condensate strengths.  $I_{crit}$  increases with both condensate strength and channel length  $L$ . However, for a given condensate strength, the critical current *density* remains roughly constant in terms of an effective channel length  $L_{eff}$ , which allows for transition regions to form the condensate.

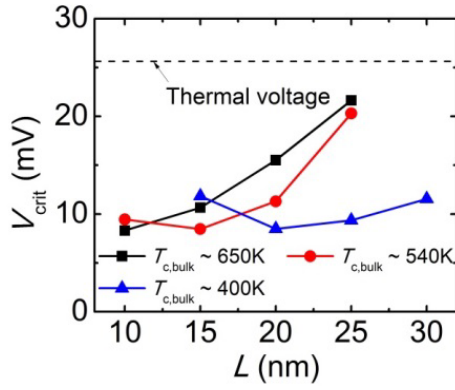


Fig. 6. Extracted critical voltages for different channel lengths and condensate strengths. U-shape curve results from the  $L$  dependencies of  $G_{ii}$  and  $I_{crit}$  as discussed in the text and shown in Figs. 4 and 5, respectively.

difference lies in the difference between “normal” current flow about the Fermi level and “supercurrent” flow below the condensate band gap, where the former launches the latter in a process akin to Andreev reflection at the interface of conventional normal conductors and superconductors [13].

#### IV. CONCLUSION

Using our atomistic tight binding quantum transport simulator including the non-local Fock exchange interaction [11], we simulated transport within a superfluid condensate with dielectrically separated layers of graphene, as to be employed for the proposed BiSFET [1]. We showed that the region required to fully form a condensate decreases with increasing bulk condensate strength; that, however, *fully* forming the condensate is optimal but not necessary for greatly enhanced interlayer conductance; that the critical interlayer current *density* is roughly effective-channel-length-independent, but increases with increasing condensate strength (in addition to bare coupling strength); that the interplay of interlayer conductance and critical current produces a more complex dependence of the critical voltage on channel length; and that a fully formed condensate blocks “normal” current flow through the condensate region.

#### ACKNOWLEDGMENT

This work was supported by the Semiconductor Research Corporation (SRC)’s Nanoelectronics Research Initiative (NRI). Supercomputing resources were provided by the Texas Advanced Computing Center (TACC).

#### REFERENCES

- [1] S. K. Banerjee, L. F. Register, E. Tutuc, D. Reddy and A. H. MacDonald, “Bilayer pseudospin field-effect transistor (BiSFET): A proposed new logic device”, *IEEE EDL* **30**, 158-160 (2009).
- [2] I. B. Spielman, J. P. Eisenstein, L. N. Pfeiffer and K. W. West, “Resonantly enhanced tunneling in a double layer quantum Hall ferromagnet”, *Phy. Rev. Lett.* **84**, 5808-5811 (2000).
- [3] E. Tutuc, M. Shayegun and D. A. Huse, “Counterflow measurements in strongly correlated GaAs hole bilayers: Evidence for electron-hole pairing”, *Phy. Rev. Lett.* **93**, 036802 (2004).

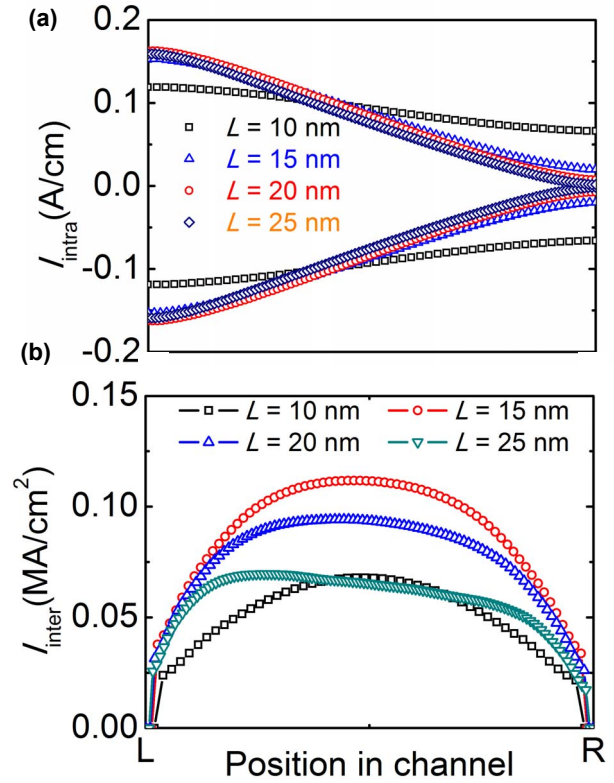


Fig. 7. (a) Intra- and (b) inter-layer current distributions. In (a) left-going currents in the top and bottom layers correspond to  $I_{intra} > 0$  and  $I_{intra} < 0$ , respectively. Position is normalized to the respective channel lengths  $L$ .

- [4] D. Nandi, A. D. K. Finck, J. P. Eisenstein, L. N. Pfeiffer and K. W. West, “Exciton condensation and perfect Coulomb drag”, *Nature* **488**, 481-484 (2012).
- [5] J. P. Eisenstein and A. H. MacDonald, “Bose–Einstein condensation of excitons in bilayer electron systems”, *Nature* **432**, 691-694 (2004).
- [6] H. Min, R. Bistritzer, J.-J. Su and A. H. MacDonald, “Room-temperature superfluidity in graphene bilayers”, *Phys. Rev. B* **78**, 121401 (R) (2008).
- [7] I. Sodemann, D. A. Pesin and A. H. MacDonald, “Interaction-enhanced coherence between two-dimensional Dirac layers”, *Phys. Rev. B* **85**, 195136 (2012).
- [8] Private communication with A. H. MacDonald
- [9] D. Basu, L. F. Register, D. Reddy, A. H. MacDonald and S. K. Banerjee, “Tight-binding study of electron-hole pair condensation in graphene bilayers: Gate-control and system-parameter dependence”, *Phys. Rev. B* **82**, 075409 (2010).
- [10] D. Basu, L. F. Register, A. H. MacDonald and S. K. Banerjee, “Effect of interlayer bare tunneling on electron-hole coherence in graphene bilayers”, *Phys. Rev. B* **84**, 0354489 (2011).
- [11] X. Mou, L. F. Register and S. K. Banerjee, “Quantum transport simulation of Bilayer pseudoSpin Field-Effect Transistor (BiSFET) with tight-binding Hartree-Fock model”, *SISPAD 2013*, 420-423, Glasgow, Scotland, United Kingdom (2013).
- [12] X. Mou, L. F. Register and S. K. Banerjee, “Quantum transport simulations on the Feasibility of the Bilayer pseudoSpin Field-Effect Transistor (BiSFET)”, *IEDM 2013*, 4.7.1-4.7.4, Washington DC, United States (2013).
- [13] X. Mou, L. F. Register and S. K. Banerjee, “Bilayer pseudoSpin Junction Transistor (BiSJT): A new ‘Beyond-CMOS’ logic device”, *IEDM 2014* (Submitted).